PAPER

Finely tuned water structure and transport in functionalized carbon nanotube membranes during desalination†

Lanlan Qin [ID] and Jian Zhou [ID] *

Molecular dynamics simulations were performed to tune the transport of water molecules in nanostructured membrane in a desalination process. Four armchair-type (7,7), (8,8), (9,9) and (10,10) carbon nanotubes (CNTs) with pore diameters around 1 nm were chosen, their interior surfaces were modified with −OH, −CH$_3$ and −F groups. Simulation results show that water transport in nanochannel depends on confined water structures which could be regulated by precisely controlled channel diameter and chemical functionalization. Increasing CNT diameter changes water structures from single-file-like to be square and hexagonal-like, then into a disordered pattern, resulting in a concave-shaped trend of water permeance. The −OH functional groups promote structural ordering of water molecules in (7,7) CNT, but disrupt water structures in (8,8) and (9,9) CNTs, and reduce the order degree of water molecules in (10,10) CNT, moreover, exert an attraction to enhance surface friction inside channel. The −CH$_3$ groups induce more strictly single-file movement of water molecules in (7,7) CNT, turning water structures in (8,8) and (9,9) CNTs into two and triangular column arrangements, improving water transport, however, causing again square-like water structure in (10,10) CNT. Fluorinations of CNT make water structure more disordered in (7,7), (9,9) and (10,10) CNTs, while enhance the square water structure in (8,8) CNT with a lower water permeance. Through changing channel diameter and functionalization, the low tetrahedral order corresponds to a more single-file-like water structure, associated with rapid water diffusion and high permeability; an increase in tetrahedrality results in more ice-like water structures, lower water diffusion coefficients, and permeability. The results of this study demonstrate that water transport could be finely regulated *via* a functionalized CNT membrane.

Introduction

Nowadays, four billion people are suffering from severe water scarcity globally.[1–3] Membrane-based technologies, enabling efficient and energy-saving separation processes, play a tremendous role in addressing this challenge.[4,5] Reverse osmosis (RO) is the most common membrane technique for desalination that allows the passage of water but blocks ions. However, the RO membranes currently used in factories are prone to be fouled, and suffer from small water flux and low desalination capacity.[6,7] Recently, biological protein channels have attracted a considerable amount of attention for potential applications in water desalination due to the ultra-high water conduction rate and high selectivity of ions.[8–10] Nonetheless, due to the structural complexity and environmental sensitivity, it is difficult to preserve the integrity and maintain their activity

at high-salinity and high-pressure conditions, or to scale up for industrial uses.[11,12] Within this context, developing biomimetic artificial channels is proposed to restore the function of biological channels and expand the application range for RO desalination through mimicking the structure of biological channels.[13–20]

Carbon nanomaterials, such as flat-sheet graphene and carbon nanotubes, are good candidates to assemble the artificial channels and replicate the structural features of biological membrane channels due to the inherent sub-nanometre size, hydrophobicity and atomically smooth tube walls.[14,21] Computer simulations and experimental studies demonstrated the extraordinarily high water permeability in carbon nanotube porins (CNTPs) with a single file water movement which was considered as the water conducting property of biological aquaporins (AQPs).[14] He *et al.*[22] designed the graphene nanopores functionalized by four carbonyl groups and four carboxylate groups which could preferentially conduct K$^+$ over Na$^+$ by mimicking the selectivity filter of KcsA K$^+$ and NavAb Na$^+$ channels. Moreover, the ion selectivity of a smaller graphene pore containing three carboxylate groups could be tuned by changing the magnitude of the applied voltage bias. Inspired by

School of Chemistry and Chemical Engineering, Guangdong Provincial Key Lab for Green Chemical Product Technology, South China University of Technology, Guangzhou 510640, P. R. China. E-mail: jianzhou@scut.edu.cn

† Electronic supplementary information (ESI) available. See DOI: https://doi.org/10.1039/d4ra01217h

the characteristic structural features of Thermotoga maritime (TmCorA) Mg^{2+} channels, Zhu et al.[23] proposed two functionalized graphene nanopore models containing five carbonyl groups and five carboxylate groups, and found both nanopores exhibited a stronger preference to Mg^{2+} than Li^+; Mg^{2+}/Li^+ selectivity ratio was higher in the carboxylate-functionalized nanopore.

As for water transport, the molecular dynamics (MD) simulations demonstrated that water spontaneously arranged into a single-file manner when confined in CNT with a diameter below 0.86 nm, whereas in a disordered state in wider CNTs. Moreover, there existed a critical size of CNT that could change water to an ice-like state.[24] Jung et al.[25] attained the enthalpy, entropy and free energy through MD simulations of water confinement in CNTs with diameters from 0.8 nm to 2.7 nm. It was discovered that water inside CNTs with diameters ranging from 0.8 to 1.0 nm had a vapor-like phase with the maximum entropic gain, whereas in CNTs with diameters of 1.1–1.2 nm, an ice-like phase with lower entropy was observed, and in CNTs with diameters larger than 1.4 nm, a bulk-like water phase was exhibited. These demonstrate that water orientations and motions inside CNT may be qualitatively modulated by adjusting the nanochannel size. Furthermore, CNT membrane–water interaction, volume fraction of CNT, as well as the eccentricity and bending also had a significant effect on water flow.[26–28]

Shen et al.[29] demonstrated that trapping single-file water chains, the synthetic aquafoldamer-based water channel was able to conduct superfast water transport at $\sim 3 \times 10^9$ H_2O per s per channel, 50% of aquaporin Z's capacity, also with a high rejection of NaCl and KCl. Song et al.[16] reported the single-file water permeation through peptide-appended hybrid[4]arene architectures with a ultrahigh transport rate of $>10^9$ H_2O per s per channel. Yuan et al.[17] also found that water molecules preferentially flow in single-file, branched chains in the porous organic cages with a fast water permeation of 10^9 H_2O s^{-1}. However, the hydroxyl channels self-assembled from octyl-ureido-polyol building blocks could generate transient cluster water pathways and achieve the same order of magnitude of water transport rates as that in AQPs.[19] Roy et al.[20] devised the polymeric channels, derived from a fully hydrogen-bonded, helically folded pore-forming hydrazide backbone; they found that the channel with a cavity of 4.3 Å and featuring a water cluster conduction mode exhibited the ultrahigh single-channel water permeability of 2.7×10^{10} H_2O s^{-1}, an improvement of 45% over that of AQP1,[30] and even higher than that of CNTPs.[14] These demonstrate that the water conduction rate in channels would be associated with the transport mode of water molecules inside channels.

In terms of water desalination, the critical CNT diameter is 0.81 nm for the complete rejection of Na^+ and Cl^- ions by MD simulations.[31] However, it would be technically challenging for the precise control of CNT diameter and synthesis in mono-chiral form at the large scale. Functionalization of CNTs or addition of functional groups to mimic the structures of AQP channels could be an effective strategy to tailor ion selectivity,[32–34] whereas these could in turn change water translocation event and influence water transport rate. Günay

et al.[35] reviewed the functionalized nano-porous membranes used or designed for desalination and water treatment. Mahdizadeh et al.[36] found the 100% salt rejection for both (6,6) and (7,7) CNT membranes. Yang et al.[37] discovered that modification of (13,13) CNT with charged functional groups ($-CH_2COO^-$ and $-CH_2NH_3^+$) enabled complete salt rejection and high water conduction, and altering the positions of functional groups could further enhance water flux. The promotion of desalination performance by modification of CNT interior with charged groups of $-COO^-$ or $-NH_3^+$ was also reported by Ding et al.[38] Moreover, under electric fields, the cations and anions exhibited distinct dynamic behaviours in positively and negatively CNTs.[39]

Considering that CNTs are also the convenient membrane-based systems for studying the nano-fluidic transport,[40,41] in this work, the CNT channels with the diameter of 0.949–1.35 nm were used and the interior surface were modified with functional groups to exquisitely tune the partitioning of water into channels. The MD simulations were performed to study the permeation events of water molecules through CNT channels in a desalination process. The transport behaviours of water molecules and water structures inside CNT channels were investigated. The results of this study indicate that the transport of water molecules within nanochannels depends on the structure of water, which can be modulated precisely by controlling CNT diameter and chemical functionalization. Decreasing the tetrahedral order of water molecules results in more single-file water structures, corresponding to rapid water diffusion and high permeability; an increase in water tetrahedrality leads to more ice-like water structures, correlating with lower water diffusion coefficients and permeability. This work could assist our understanding of water transport mechanisms through nanochannels.

Simulation method

Molecular design

As demonstrated by Jung et al.,[25] water state in CNTs with diameters of 0.8–1.4 nm would experience a change from a vapor-like phase, an ice-like structure and a bulk-like phase. Therefore, the armchair (7,7), (8,8), (9,9) and (10,10) CNTs with diameters of 0.949 nm, 1.08 nm, 1.22 nm and 1.35 nm, were chosen to investigate water transport in a simulated RO desalination process.

To modulate water structures in channels, three typical functional groups, hydroxyl (–OH), methyl ($-CH_3$) and fluorine (–F), were used to modify the interior surface of CNTs, as shown in Fig. 1a. The –OH group, which can act as both hydrogen bonds (H-bonds) donor and acceptor, has a natural affinity with water molecules, so –OH groups can change the orientation and arrangement of water molecules through hydrogen bonding. The $-CH_3$ group is hydrophobic and chemically inactive, which can exert a hydrophobic force on water molecules and trigger molecular reorientation. The fluorine group (–F), inherently amphiphobic with low surface energy,[42,43] can exhibit some unique characteristics and may initiate quite different transport behaviours of water molecules through nanochannels.
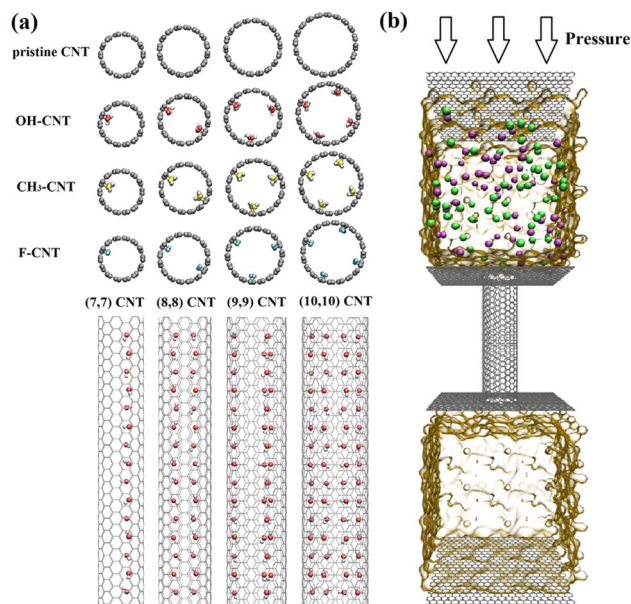
Fig. 1 The top view of pristine and functionalized CNT channels and front view of OH-CNT channels (a); simulation system for water desalination through CNT channels (b). Different atoms are shown with different colors, Na^+: purple, Cl^-: green, C: grey, O: red, H: white, F: cyan. The carbon atoms in $-CH_3$ groups are colored in yellow.

Besides, addition of two $-CH_3$ groups in the cross-section of (7,7) CNT will cause the complete pore closing for water molecules, therefore, only one $-CH_3$ group was added. To be consistent, the (7,7) CNT was also modified with one $-OH$ or $-F$ group in the cross-section to construct OH-(7,7) CNT and F-(7,7) CNT model. In the axial direction (z direction), the functional groups were added per three sp^2 carbon atoms with a vertical distance of 0.369 nm to avoid the interactions between the modifying groups, so there were fifteen functional groups in axial direction. For (8,8), (9,9) and (10,10) CNTs, their cross-sections were uniformly modified with two, three and four functional groups, respectively, to make the effective pore diameter be more comparable to that of (7,7) CNT. Therefore, thirty, forty-five and sixty groups existed inside functionalized (8,8), (9,9) and (10,10) CNT channels, respectively, as seen in Fig. 1a, taking the OH-CNT as an example.

Setup of model

To simulate water transport through CNT channels with different functional groups in a desalination process, a 5.4 nm-long CNT inserted between two graphene plates of size 5.09×5.04 nm^2 was used to form transmembrane channel, as shown in Fig. 1b; a hole of the similar size as CNT diameter was drilled in the center of graphene plates to allow water transfer through channels. Two boxes containing NaCl solution and pure water with the thickness of 6.5 nm were separated by CNT channels. The saline box contains 4683 water molecules, 53 Na^+ and 53 Cl^-, corresponding to NaCl concentration of 0.6 M which is close to the salt concentration in seawater. The pure water box contains 4789 water molecules. Additionally, two perfect

graphene plates were introduced into the end of two boxes. The two-dimensional periodic boundary (2D PBC) systems referred to the ref. 44 were adopted, that the length in the z direction of the simulation systems was set to 34 nm for making the contribution of repeat units in this direction negligible. A force along $-z$ axis direction was applied on the upper graphene and 1 bar pressure along $+z$ axis was applied on the bottom graphene. The transmembrane pressures ΔP applied between two graphene plates was set as 100 bar.[45]

Simulation details

The Gromacs 2019.6 package[46] was employed to simulate water desalination process. OPLS-AA force field[47] was used for all the simulation system and SPC/E model[48] was employed to describe water molecules. The Lennard-Jones (LJ) potentials for cross interactions between different atoms were calculated by the Lorentz–Berthelot combining rule. The long-range electrostatic interaction was calculated with the Particle Mesh Ewald (PME)[49] method, the cut-off distance was set to be 1.2 nm. The Nosé–Hoover method[50] was used to couple the temperature at 300 K. Initially, the systems were energy-minimized using the steepest descent method, and then pre-equilibrated for 2 ns in an NVT ensemble. Afterward, a 100 ns non-equilibrium production simulation was conducted. When the numbers of water molecules permeating through CNT membranes exhibit a linear change over simulation time, it is regarded as achieving a steady-state of water flow. The time step was set to be 2 fs. For each system, the simulation processes were repeated for 3–5 times. The trajectories were recorded at every 20 ps for analysis.

Results and discussion

Water structures in CNTs

The top and front views of the structures of water molecules transport through different CNT membranes were shown in Fig. 2. It was observed in Fig. 2a that water molecules exhibit a single-file-like chain structure locally in the pristine (7,7) CNT membrane; meanwhile, they are also distributed in two columns at localized positions. Introduction of $-OH$ groups inside (7,7) CNT membrane causes water molecules arrangement in two columns more remarkable, which is due to the attraction of $-OH$ to water molecules. In CH_3-(7,7) CNT membrane, water molecules are in a stricter single-file arrangement compared with that in pristine (7,7) CNT. Water molecules inside F-(7,7) CNT membrane are also in both single and double chains arrangements (Fig. 2a).

As seen in Fig. 2b, in pristine (8,8) CNT membrane, water molecules display an array with four rectangular columns and form square-like structures, which is consistent with the finding in ref. 51. Such highly structured water arrangement demonstrates the properties of high viscosity[52] and low diffusibility[53] of confined water, which would substantially impede water transport. While $-OH$ functionalization destroys the 4-gonal square structures of water molecules, a similar pentagonal geometry is formed. The symmetrical two-column structures were formed for water molecules in CH_3-(8,8) CNT membrane.
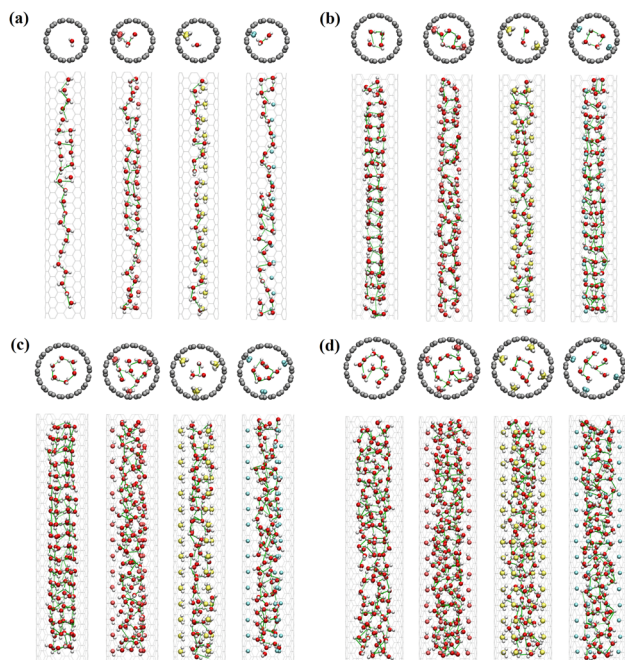
Fig. 2   Top and front views of water molecules in CNT membranes: (a) (7,7) CNT; (b) (8,8) CNT; (c) (9,9) CNT; (d) (10,10) CNT. Each subfigure in the diagram, from left to right, represents pristine CNT, OH-CNT, CH$_3$-CNT and F-CNT correspondingly. The green dash lines represent HB bonds between water molecules.

However, the water structures become more rectangular in F-(8,8) CNT membrane compared with that in pristine (8,8) CNT, which means that the ordered structure of water molecules is intensified, which may further hinder water transport.

As can be seen in Fig. 2c, a hexagonal structure of water molecules is found in pristine (9,9) CNT membrane. This kind of water structure exhibits many similar properties as the square water structures,[51] so water molecules may have an extremely low transfer rate in (9,9) CNT membrane. Modification of membrane with –OH, –CH$_3$ and –F, all disrupt the hexagonal structure and make water molecules arranged in a more irregular way. Concretely, some water molecules even appear in the centre of channel, forming a similar two-layer ring structure in both OH-(9,9) CNT and F-(9,9) CNT membranes; while water molecules exhibit a triangular distribution in CH$_3$-(9,9) CNT membrane (Fig. 2c). Comparatively, two layered water structures are formed in pristine (10,10) CNT membrane with one water layer near membrane wall and another layer located at the centre. After –OH and –F functionalization, the layered water structures in CNT channel become blurry. However, in CH$_3$-(10,10) CNT membrane, water structures again become square-like. The above results demonstrate that water structure could be significantly altered by channel diameter and chemical functionalization.

Water density inside CNTs

To understand the water transport mechanism through nano-structured CNT membranes, the density distribution of water

molecules in CNTs along the z-axis are analysed and plotted in Fig. 3 with the average water density values listed in the inset tables. The centre of CNT membranes is located at $z = 0$; $z > +2.5$ nm represents water entering CNT channels from saline water whereas $z < -2.5$ nm refers to water passing through CNTs, corresponding to the water molecules flowing from top to bottom in Fig. 1b. As can be seen from Fig. 3a that the density profile of water molecule in pristine (7,7) CNT membrane along the axial direction is close to a straight line, the average water density value is equal to 5.53 kg m^{-3}, which is two orders of magnitude lower than the water density in bulk solution, 982.6 kg m^{-3}. Zhou et al.[54] found that the diffusion of molecules confined in a slit pore strongly depend on the density. Köhler and Silva[55] found a strong dependence between the density of water and its viscosity, and the viscosity of confined water is about an order of magnitude lower than bulk solution and decreases with decreasing CNT diameter. The gas-like phase of water molecules in CNTs with a 0.8–1.0 nm has also been mentioned in ref. 25. Therefore, the low viscosity of water molecules may cause a high-water transfer rate in (7,7) CNT.

Modification of (7,7) CNT inner surface with –OH groups slightly increases pore water density, that the average water density in OH-(7,7) CNT is 6.97 kg m^{-3}. This is due to the hydrophilic nature of –OH groups, which attract water molecules through hydrogen bonding,[56] thus resulting in more water molecules in the channel. Moreover, Wei et al.[57] demonstrated that the hydrogen bond (HB) network would reduce the diffusivity of water through the slits, as such, –OH groups functionalization may suppress water transport. In contrast, –CH$_3$ groups lead to a reduced water density with the average value of 5.03 kg m^{-3} owing to the geometric steric effect.[58] The density of water in F-(7,7) CNT, 5.65 kg m^{-3}, is marginally larger than that in pristine (7,7) CNT. From Fig. 3b, the average water density inside pristine (8,8) CNT membrane is equal to 16.1 kg m^{-3}. Modification with –OH groups causes an undulated density profile along the axial direction with a smaller average water
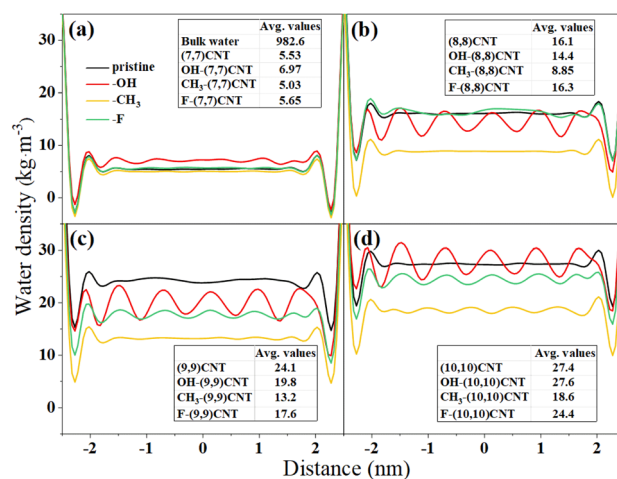

Fig. 3   The density distributions of water molecules in CNT membranes along the z axis: (a) (7,7) CNT; (b) (8,8) CNT; (c) (9,9) CNT; (d) (10,10) CNT.

density of *ca.* 14.4 kg m^{-3}. This is because water molecules are concentrated near –OH groups by HBs, resulting in a local enhancement and a fluctuated distribution, which would enhance the friction force.[59] In CH$_3$-(8,8) CNT membrane, the water density is reduced to half of that in pristine (8,8) CNT, 8.85 kg m^{-3}, while water density in F-(8,8) CNT is slightly increased, 16.3 kg m^{-3}.

For pristine (9,9) CNT membrane, water density is elevated to *ca.* 24.1 kg m^{-3} (Fig. 3c). Addition of –OH, –CH$_3$ and –F groups at inner surface all cause a reduction in water density. Identically, a fluctuated density profile was observed in OH-(9,9) CNT with a smaller density value of 19.8 kg m^{-3}. Water densities in CH$_3$-(9,9) CNT and F-(9,9) CNT are decreased to 13.2 and 17.6 kg m^{-3}, respectively. As shown in Fig. 3d, water density in pristine (10,10) CNT membrane is *ca.* 27.4 kg m^{-3}. In OH-(10,10) CNT, the average water density is slightly larger, 27.6 kg m^{-3}, also with an uneven distribution. In contrast, both –CH$_3$ and –F functionalization result in a lower water density, that the average values are 18.6 and 24.4 kg m^{-3} in CH$_3$-(10,10) CNT and F-(10,10) CNT, respectively.

Water orientation and hydrogen bonds formed inside CNTs

It had been reported that water orientation could significantly influence water mobility and alter water conduction process.[60,61] CNT channels are divided into slices with the thickness of 0.25 nm which is approximately the diameter of one water molecule.[62,63] The average orientation angle θ between the dipole moment of water and z-axis in each slice was calculated. The water orientation results were attained by further averaging the θ values by the slices, as shown in Fig. 4a. The number of water molecules in the cross-section of all CNT membranes was analysed, the results were presented in Fig. 4b. Hydrogen bonding between water molecules plays an important role in determining water structure, stability and properties. The average number of HBs formed per water molecule inside CNT membranes were calculated as shown in Fig. 4c. A geometrical criteria of hydrogen bond was employed in this work, *i.e.*, the

distance between donor and acceptor atoms is smaller than 0.35 nm and the angle hydrogen-donor–acceptor is less than 30°.[64,65] The HB network structures for water molecules in CNT membranes were also displayed in Fig. 2.

As seen in Fig. 4a, water molecules in pristine (7,7) CNT exhibit a preferred orientation with the θ of 141.9° between the dipole and z axis. That θ close to zero or 180° indicates an axial orientation of water molecule, and the value approaching 90° indicates a perfect radial orientation. The high θ demonstrates a predominant axial orientation of water molecules in pristine (7,7) CNT. From Fig. 4b, the average number of water molecules in cross-section of pristine (7,7) is approx. 1.33, implying that one water molecule exists in the cross-section. Moreover, it was observed that the average HB number formed per water molecule is 2.18 (Fig. 4c), close to 2, which means that one water molecule forms two HBs on average. According to Fig. 2a, in most positions of pristine (7,7) CNT, the water molecule forms a HB with both the upper and lower axial water molecules, presenting a similar transport mode of single-file water chain in biological AQPs.[8,10]

Addition of –OH group inside (7,7) CNT causes the average θ for water dipole with z axis reduce to 95.8°, so water molecules have a more radial orientation. The number of water molecules in the cross-section and the number of HB bonds formed per water molecule increase to 1.69 and 2.29, respectively. As seen in Fig. 2a, more water molecules could form HBs with both the neighbouring axial and radial water molecules. It was demonstrated that the hydrogen bonding between water and neighbouring water molecules plays an important role in water dynamics.[66] The increased number of HBs between water molecules would decrease the mobility of water and reduce water transport in OH-(7,7) CNT.

In contrast, in CH$_3$-(7,7) CNT membrane, the average θ between water dipole and z axis is 142.6°, slightly larger than that in pristine (7,7) CNT, indicating a more axial water orientation. The number of water molecules in the cross-section and HBs formed per water molecules are decreased to 1.20 and 2.10, respectively, which is attributed to the geometric restriction and hydrophobic nature of –CH$_3$ groups.[58,67] In Fig. 2a, the nearly straight HB network in the axial direction in CH$_3$-(7,7) CNT was observed. The reduced HB number formed per water molecule in CH$_3$-(7,7) CNT membrane may enhance water mobility and be favourable for water transport. In F-(7,7) CNT membrane, water molecules are oriented in a direction with the dipole moment having an orientation angle of 97.9° with the z axis. The number of water molecule in the cross-section (1.37) and the average number of HBs (2.23) that each water molecule forms with the neighbouring water molecules are also both slightly increased. The HB network also resembles a line for water molecules in most locations within F-(7,7) CNT.

For water molecules in pristine (8,8) CNT membrane, the average θ between water dipole and z axis is close to 90°, that water dipole moment is perfectly aligned perpendicular to the axial direction. The average number of water molecules in the cross-section is 3.87, close to 4, as shown in Fig. 4b, which make water molecules easily form a square structure. The number of HBs per water molecule is *ca.* 3.56, demonstrating that each
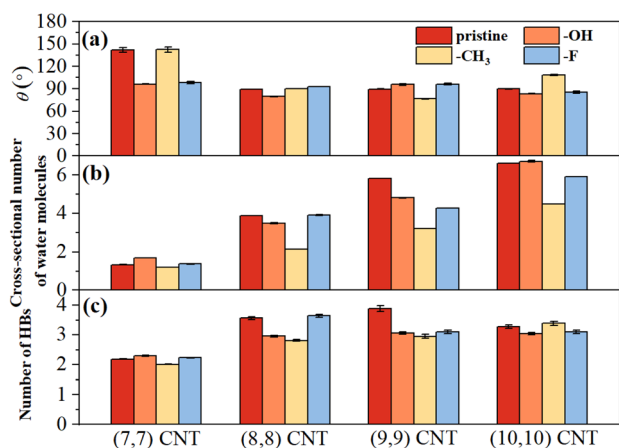

Fig. 4 Average dipole orientation angles θ of water molecules (a), number of water molecules in the cross-section (b), and number of HBs formed per water molecule (c) in different CNT membranes.

water molecule at the corners of the quad can form HBs not only with the adjacent two water molecules at the corners, but also with water molecules in axial direction. In Fig. 2b, it was observed that the HB network of water molecules is like a square tube in pristine (8,8) CNT. Koga *et al.*[68] also found the formation of solid-like square tube water structure inside CNT. Comparatively, –OH groups functionalization causes water dipole slightly shifted toward the axial direction with the average θ being 79.9°. The number of water molecules in cross-section is decreased to 3.49, demonstrating that the ordered water structure may be disrupted. Moreover, the average number of HBs for water molecule with the neighbouring water molecules is reduced to 2.95, indicating improved water mobility, which may contribute to water transfer. Fig. 2b also shows the less ordered HB network structure in OH-(8,8) CNT membrane.

In CH$_3$-(8,8) CNT, although the average θ for water dipole with z axis is also close to 90° (Fig. 4a), the average number of water molecules in cross-section is only 2.13, which means that only two water molecules exist in the cross-section, so it is incapable of developing the square-like structure. The mean number of HBs formed per water molecule further declines to 2.81, and the HB network shows a two-dimensional mesh structure. Functionalization of (8,8) CNT with –F groups induces water dipole being a slightly larger θ, 92.5°, with z axis. The number of water molecules in cross-section and HB number per water molecules are both increased, 3.90 and 3.64, respectively. In Fig. 2b, the square tube water structure was also observed in F-(8,8) CNT, moreover, the HB network in the cross-section is more rectangular, meaning that the ordered square structure is further enhanced, which would be unfavourable for water transport.

According to Fig. 4a and b, the average θ for water molecules in pristine (9,9) CNT membrane is also *ca.* 90° and the average number of water molecules in cross-section is close to 6, which mean that a hexagonal water structure could be formed. From Fig. 4c, the average number of HBs per water molecule is *ca.* 4 in pristine (9,9) CNT. As seen in Fig. 2c, water molecule forms HBs with both the water molecules in the cross-section and axial direction, generating a hexagonal tube-like HB network. Other studies[69,70] had also reported this hexagonal water structure in (9,9) CNT, which exhibited ice-like behaviour and very low diffusion capability. In OH-(9,9) CNT, the average θ between water dipole with z axis is *ca.* 95.4°. The average numbers of water molecules in cross-section and HBs formed per water molecules are reduced to 4.81 and 3.06, respectively, which means the breakage of hexagonal water structure. In Fig. 2c, disordered HB network was observed in OH-(9,9) CNT.

Functionalization with –CH$_3$ groups causes a more axial water orientation, that the θ between water dipole and z axis is 76.6°. Moreover, the number of water molecules in cross-section is close to 3, meaning triangular arrangement. From Fig. 4c, the average number of HBs for water molecule with its neighbouring water molecules is further reduced to *ca.* 2.95. As shown in Fig. 2c, the HB network exhibits a rough triangular column structure in CH$_3$-(9,9) CNT but with no triangle HB network formed in the cross-section. In F-(9,9) CNT membrane, the average θ for water dipole with z axis becomes larger, 96.1°.

Similarly, both the average number of water molecules in cross-section and the average number of HB formed per water molecule were decreased with the values being 4.27 and 3.10, respectively, also indicating the disruption of the hexagonal structure of water molecules. Correspondingly, in Fig. 2c, the irregular HB network in F-(9,9) CNT was observed.

Water molecules in pristine (10,10) CNT membrane also exhibit a radial orientation with the dipole perpendicular to z axis. The average number of water molecules in cross-section rises to 6.62; however, the average number of HBs per water molecules is decreased to 3.28, indicating the improved water mobility. In Fig. 2d, the HB network in pristine (10,10) CNT displays a disordered structure. Functionalization of (10,10) CNT with –OH groups yields a more axial water orientation with the average θ of 83.3° for water dipole with z axis. The number of water molecules in cross-section is slightly increased, 6.71, but with a lower HB number per water molecule. Also, a disordered HB network in OH-(10,10) CNT was observed.

In CH$_3$-(10,10) CNT, the average θ for water dipole with z axis is 108.1°. The average number of water molecules in cross-section is reduced to 4.50. Surprisingly, the average HB number per water molecules is even larger (3.38) than that in pristine (10,10) CNT, which could decrease water mobility. In Fig. 2d, there is a square-like HB network in CH$_3$-(10,10) CNT. Addition of –F groups causes a smaller θ for water dipole with z axis. The average number of water molecules in cross-section and the average HB number formed per water molecule decline to 5.92 and 3.10, respectively. The disordered HB network was also seen in F-(10,10) CNT membrane (Fig. 2d).

As can be seen from the above results, the CNT diameter has a significant impact on the structure of confined water molecules. With the increase in CNT diameter, the structure of confined water transits from a single file pattern to square and hexagonal, and eventually adopts a disordered mode. The influence of CNT diameter and functional group modification (including modification quantity) on water structure is extremely complex: for CNTs with different diameters, the modification of the same functional group may exhibit varying effects, and conversely, different functional group modifications on CNT of the same diameter may lead to diverse outcomes. The –OH functionalization induces a more radial orientation of water molecules in (7,7) CNT, but disrupts the square and hexagonal water structures in (8,8) and (9,9) CNTs, as well as blurs the layered water structure in (10,10) CNT. The –CH$_3$ groups cause a more stringent linear distribution of water molecules in CH$_3$-(7,7) CNT. Although it also breaks down the ordered structures of water molecules in (8,8) and (9,9) CNTs, it paradoxically leads to an ordered square structure in CH$_3$-(10,10) CNT. Functionalizing –F groups results in a roughly linear distribution of water molecules in F-(7,7) CNT, creating more disordered water structures in F-(9,9) and F-(10,10) CNTs, yet strengthening the square structure of water molecules in F-(8,8) CNT.

Water order parameter

To identify the local arrangements of water molecules when transport within different CNT membranes, based on the

coordinates of the oxygen atoms, the tetrahedral order parameter was calculated. It could be used to distinguish ice-like and liquid-like water molecules,[71] such as hexagonal ice. For each water molecule, the tetrahedral order parameter q is defined as[72]

$$q = 1 - \frac{3}{8}\sum_{j=1}^{3}\sum_{k=j+1}^{4}\left(\cos\psi_{jk} + \frac{1}{3}\right)^2 \qquad (1)$$

where q is computed from a sum over the four nearest neighbours of water molecule. ψ_{jk} is the angle formed by oxygen atoms of the central water molecule and its nearest neighbours j and k (≤ 4). The range of possible values for q is between -3 and 1. When the four neighbouring molecules form a perfect tetrahedral arrangement around the central molecule, i.e., ψ_{jk} of 109°28′, q is equal to 1. The value of q is negative when the four nearest neighbours adopt a linear-like configuration (i.e., single-file). The average value of q measures the degree of tetrahedrality in the system. For an uncorrelated system (ideal gas case), $\langle q \rangle = 0$ (where $\cdots$ denotes an ensemble average); while for a perfect tetrahedral network, $\langle q \rangle = 1$.

The probability distribution of q for water molecules within different CNT membranes are shown in Fig. 5 and the average values of q for each system are listed in the inset tables. As seen in Fig. 5a, the calculated average value of q for bulk water is 0.421, demonstrating a tetrahedral environment. In pristine (7,7) CNT membrane, the distribution curve exhibits a distinct peak at $q = -0.25$ and the average value is -0.457, meaning that water molecules are in a linear-like configuration, that is, like a single file. The peak is shifted right to $q = -0.05$ with the average value of -0.248 in OH-(7,7) CNT membrane, which imply that more water molecules are in a tetrahedral bonding environment. Comparatively, addition of –CH$_3$ groups causes the peak left-shifted with a more negative q value, indicating more linear arrangement of water molecules. For F-(7,7) CNT membrane, the peak height is slightly reduced and the average value of q becomes smaller, -0.461, demonstrating the less tetrahedral bonding environment.

As seen in Fig. 5b, a significant peak at $q = 0.61$ was observed in the distribution curve for pristine (8,8) CNT membrane. The calculated average value of q is 0.462, which is even larger than that of bulk water, indicating the high tetrahedrality of water molecules in (8,8) CNT. This is due to the formation of square-like water structure (Fig. 2b), which is a stable and highly ordered ice-like structure, therefore, exhibiting a high q value. Differently, –OH functionalization greatly reduces q and the peak moves left with the average value being 0.248, suggesting a notable decrease of tetrahedrality. In CH$_3$-(8,8) CNT, the breakage of tetrahedrality is more remarkable, that there is a large probability distribution for $q < 0$ and the average value of q is also negative, -0.121. Unexpectedly, the peak height is increased with the average value of q being 0.481 for F-(8,8) CNT, indicating the enhancement of tetrahedrality.

In Fig. 5c, a remarkably high peak located at $q = 0.61$ in the distribution curve for pristine (9,9) CNT membrane was observed, which is consistent with the result of Kong et al.'s study.[73] The average value of q is 0.531, suggesting a highly tetrahedral structure of water in pristine (9,9) CNT. The significantly high calculated q is also a result of the formation of ice-like structure (Fig. 2c), where the hexagonal water structure represents an extremely ordered arrangement. Modification with –OH, –CH$_3$ and –F groups all result in a reduction of q and wider distribution, indicating the damaged tetrahedral structure of water molecules. Particularly, the peak in the distribution curve of q for CH$_3$-(9,9) CNT even appears at the negative region. The average values of q are 0.325, 0.0877 and 0.313 for OH-(9,9) CNT, CH$_3$-(9,9) CNT and F-(9,9) CNT membranes, respectively.

For pristine (10,10) CNT membrane, a peak located at $q = 0.49$ was observed in the distribution curve with the average value (0.384) lower than that of bulk water (0.421), meaning more disordered water structure. This suggests that when the pore diameter further increases, water bulk properties become more pronounced. Therefore, the structures of water molecules do not transit progressively from a disordered state to bulk-like state as the pore size increases; instead, in this process, the highly ordered state resembling ice-like structure, exhibiting great orderliness, may emerge. Likewise, the peak heights become lower with smaller average q values, 0.338 and 0.333, respectively, after passivated with –OH and –F groups. However, for CH$_3$-(10,10) CNT membrane, there is a pronounced peak occurring at $q = 0.73$. This means the appearance of ordered water molecules in CH$_3$-(10,10) CNT membrane, which would largely hamper water transport. This effect is not reflected in the average value due to the increased distribution of q in negative region.

Based on the results above, the effects of CNT diameter and functional groups on the orderliness of water molecules are mutually correlated. Increasing the diameter of CNT does not result in a monotonic increase in the tetrahedral order of water molecules; instead, it leads to the emergence of ice-like structures, causing the order degree of water molecules in (8,8) and (9,9) CNT membranes even higher than that in bulk water. For each CNT membrane, modification with different functional groups produces varying effects on the orderliness of water
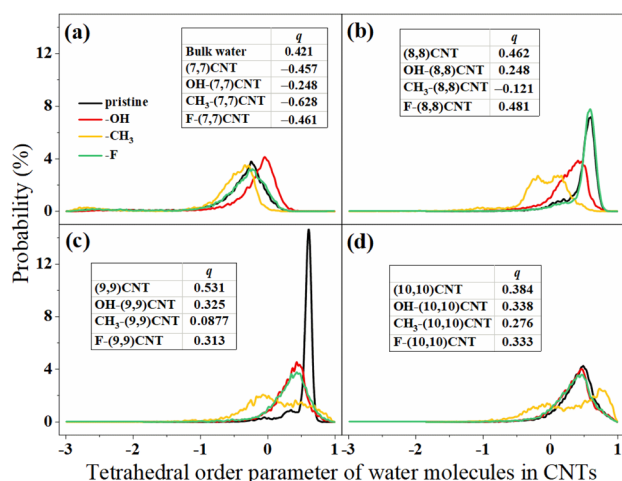

Fig. 5 Probability distributions of tetrahedral order parameter for water molecules in CNT membranes: (a) (7,7) CNT; (b) (8,8) CNT; (c) (9,9) CNT; (d) (10,10) CNT.

molecules. The –OH groups increase the tetrahedral order of water molecules in (7,7) CNT membrane, while –CH$_3$ and –F groups cause a reduction in tetrahedrality of water molecules. For (8,8) CNT membrane, on the contrary, –F modification enhances the water tetrahedral order. In the case of (9,9) CNT membrane, functionalizing –OH groups decrease the orderliness of water molecules, whereas –CH$_3$ groups lead to an increased tetrahedral order parameter in (10,10) CNT membrane. Furthermore, the effect of the same functional groups on tetrahedral order of water molecules for different CNT membranes also differs. The –OH functionalization enhances the tetrahedral order of water molecules in (7,7) CNT, but reduces the degree of tetrahedrality in (8,8), (9,9), and (10,10) CNT membranes. The –CH$_3$ groups decrease the tetrahedrality of water structure in (7,7), (8,8) and (9,9) CNT membranes but result in an increase in tetrahedral order of water molecules in (10,10) CH$_3$-CNT membranes. Fluorination of CNT reduces the tetrahedral order of water molecules in F-(7,7), F-(9,9), and F-(10,10) CNT membranes, while increases tetrahedrality of water structure in F-(8,8) CNT.

Therefore, adding functional groups into larger-diameter CNT membranes may lead to a reduction in the effective pore size, enhance the order degree of water molecules, intensifying the highly ordered water structure (F-(8,8) CNT), or reproducing the ice-like structure (CH$_3$-(10,10) CNT). On the other hand, in the CNT membranes with ice-like water structures, modification with functional groups could reduce the orderliness of water molecules, disrupt the tetrahedral structures, such as in CH$_3$-(8,8), OH-(9,9), CH$_3$-(9,9), and F-(9,9) CNT membranes. In the molecular design of artificial nanochannels such as applied in desalination or ion sieving, it is crucial to devise appropriate pore size, select suitable functional groups and modifying positions to avoid the formation of ice-like structures, or disrupt the existing ordered water structures through rational modification.

Water–water interaction

As demonstrated above, water molecules inside CNT membranes exhibit distinct water structures, therefore, the transport of water would be significantly influenced by the surrounding water molecules.[74] The water–water interaction energy is examined for a single water molecule migrating inside different CNT membranes, as shown in Fig. 6, the average values are listed in the inset tables. As seen in Fig. 6a, the interaction energy for a single water molecule with its surrounding water molecules in bulk solution is −84.1 kJ mol^{-1}. In pristine (7,7) CNT membrane, the water–water interaction curve approaches a straight line, and the interaction energy holds at about −56.3 kJ mol^{-1}, indicating the reduced water–water interaction. In OH-(7,7) CNT membrane, an undulated interaction profile was observed with an average water–water interaction energy of −54.4 kJ mol^{-1}. The number of valleys in the profile is consistent with the number of –OH groups. The water–water interaction at the valley is even stronger than that in pristine (7,7) CNT, corresponding to an increased tetrahedrality (Fig. 5a). In contrast, modification with
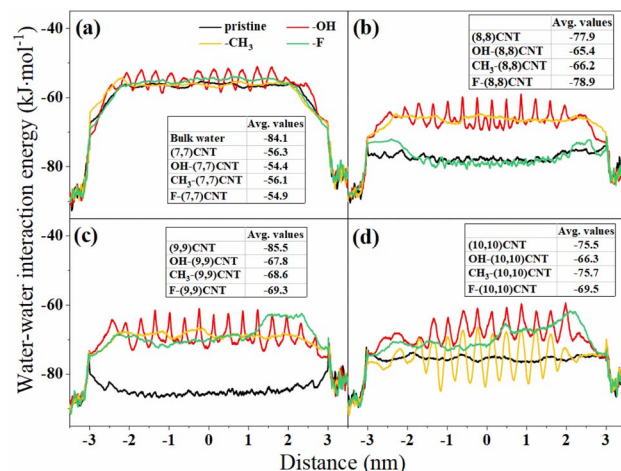

Fig. 6 Water–water interaction energies when a single water molecule passes through different CNT membranes: (a) (7,7) CNT; (b) (8,8) CNT; (c) (9,9) CNT; (d) (10,10) CNT.

–CH$_3$ and –F groups both weakens the water–water interaction with the average energies of −56.1 and −54.9 kJ mol^{-1}, respectively, which also correspond to smaller tetrahedral order values.

In pristine (8,8) CNT membrane, the average water–water interaction energy is *ca.* −77.9 kJ mol^{-1}. The water–water interactions are diminished both in OH-(8,8) CNT and CH$_3$-(8,8) CNT membranes with energy values of −65.4 and −66.2 kJ mol^{-1}, respectively. However, water–water attraction become stronger, the average interaction energy is −78.9 kJ mol^{-1} after fluorination of (8,8) CNT membrane, which is associated with larger tetrahedral order in Fig. 5b. The water–water interaction in pristine (9,9) CNT membrane (−85.5 kJ mol^{-1}) is strengthened compared with that in bulk water. Correspondingly, the tetrahedral order parameter for water in pristine (9,9) CNT is also higher than that of bulk water. Functionalization by –OH, –CH$_3$ and –F groups all weaken water–water interaction with the energy values being −67.8, −68.6 and −69.3 kJ mol^{-1}, respectively. In pristine (10,10) CNT membrane, the average water–water interaction energy is *ca.* −75.5 kJ mol^{-1}. Similarly, the water–water interaction strength weakens in both OH-(10,10) CNT (−66.3 kJ mol^{-1}) and F-(10,10) CNT membranes (−69.5 kJ mol^{-1}). However, water–water interaction is enhanced in CH$_3$-(10,10) CNT membranes with energy value of −75.7 kJ mol^{-1}, which is due to existence of ice-like water structure (Fig. 2d).

Membrane–water interaction

As demonstrated in Fig. 2, HBs could be formed between water molecules and –OH functional groups. It was reported that water transport could be affected by channel-lining functional groups.[75] Therefore, the membrane–water interaction energy was also calculated when a single water molecule passes through different CNT membranes, results are shown in Fig. 7 with average values listed in inset tables. From Fig. 7a, the interaction energy profile between pristine (7,7) CNT membrane
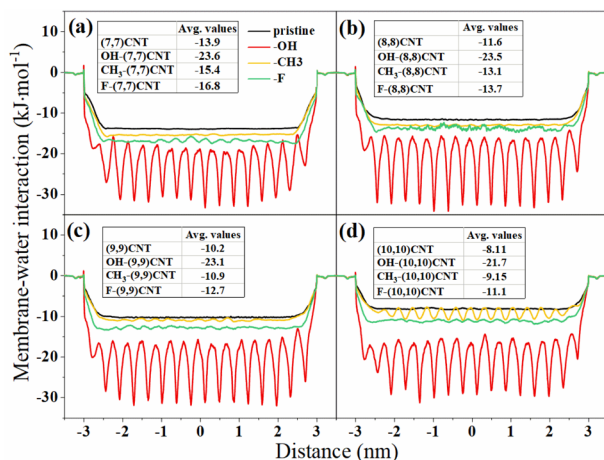
Fig. 7 Membrane–water interaction energy when single water molecule passes through CNT membranes: (a) (7,7) CNT; (b) (8,8) CNT; (c) (9,9) CNT; (d) (10,10) CNT.

and water is also close to a straight line with the average energy value of *ca.* −13.9 kJ mol^{-1}. For OH-(7,7) CNT membrane, the membrane–water interaction energy fluctuates between −33.3 and −16.9 kJ mol^{-1} with the average value of −23.6 kJ mol^{-1}. The enhanced membrane–water interaction is attributed to the affinity by –OH groups.[76,77] Wang *et al.*[26] reported that enhancing CNT membrane–water interactions would lower water flow rates and velocities. The valleys in interaction energy profile are the locations of –OH groups. In addition, the existence of –OH groups inside CNT could increase surface friction.[78–80] Therefore, –OH modification could produce adverse effect on water transport. The membrane–water interactions are slightly strengthened in both CH$_3$-(7,7) CNT and F-(7,7) CNT membranes with the average energy values of −15.4 and −16.8 kJ mol^{-1}, respectively.

As seen in Fig. 7b, the membrane–water interaction energy in pristine (8,8) CNT membrane is *ca.* −11.6 kJ mol^{-1}. The –OH functionalization also causes an undulated interaction energy profile with improved membrane–water interaction, the average energy value is −23.1 kJ mol^{-1}. Similarly, the weakened membrane–water interaction was observed in both CH$_3$-(8,8) CNT (−13.1 kJ mol^{-1}) and F-(8,8) CNT membranes (−13.7 kJ mol^{-1}). The same trends were also seen in (9,9) and (10,10) CNT-based membranes. The average interaction energy between membrane and water for a water molecule migrating inside pristine (9,9) CNT membrane is −10.2 kJ mol^{-1}. This value becomes −23.1, −10.9 and −12.7 kJ mol^{-1} for OH-(9,9), CH$_3$-(9,9) and F-(9,9) CNT membranes, respectively. Identically, membrane–water interaction energy is *ca.* −8.11 kJ mol^{-1} for pristine (10,10) CNT membrane. Introduction of –OH, –CH$_3$ and –F groups causes the membrane–water interaction energies of −21.7, −9.15 and −11.1 kJ mol^{-1}, respectively.

Interestingly, an undulating membrane–water interaction energy profile was also observed for CH$_3$-(10,10) CNT membrane. The number of peaks or valleys in the profile corresponds to the number of –CH$_3$ groups, and the –CH$_3$ groups are located at the peaks of the profile. As demonstrated

in Fig. 2d, in CH$_3$-(10,10) CNT membrane, the square-like water structures were formed at the –CH$_3$ groups modified regions, which result in a decreased intermolecular distance and strengthened interactions among water molecules (Fig. 6d). Correspondingly, the distance between water molecules and membrane increases, weakening their interactions. Conversely, in the areas where no –CH$_3$ groups are modified, water molecules exhibit relatively disordered structures, causing larger distance and weaker interactions between water molecules, whereas smaller distance and stronger interactions between water molecules and membrane. Consequently, the membrane–water interaction energy fluctuates for water molecules passing through CH$_3$-(10,10) CNT membrane.

Water residence time

Water residence time dynamics measures how long a water molecule stays in a specified region and could characterize the dynamic property of water. Water residence time can be evaluated from the correlation function $C_r(t)$:[81]

$$C_r(t) = \frac{1}{N_n} \sum_{j=1}^{N_n} \frac{\langle P_{Rj}(0) P_{Rj}(t) \rangle}{\langle P_{Rj}(0)^2 \rangle} \quad (2)$$

where $\langle \cdots \rangle$ represents the ensemble average. P_{Rj} is a binary function that takes the value of 1 if the *j*th water molecule stays in the selected region at time *t* and is equal to zero otherwise. N_n is the number of all water molecules in the selected area. By an exponential fit of $C_r(t)$ *vs.* simulation time *t*, the water residence time can be approximated:

$$C_r(t) = A_r \exp\left(-\frac{t}{\tau}\right) \quad (3)$$

where A_r is the amplitude, τ is the relaxation time, which represents the mean residence time of a water molecule in a specified region. The $C_r(t)$ curves for water in different CNT membranes were plotted in Fig. S1 of ESI.† The fitting results for water residence time τ are presented in Fig. 8. The water residence time in pristine (7,7) CNT membrane is *ca.* 1.28 ns. A larger residence time for water molecules (3.33 ns) in OH-(7,7) CNT membrane was observed, indicating the decreased water mobility. In contrast, water residence time is reduced to 1.37 and 1.01 ns in CH$_3$-(7,7) CNT and F-(7,7) CNT membranes, respectively, which implies an increased mobility of water.

In pristine (8,8) CNT membranes, water residence time is *ca.* 5.43 ns. Similarly, the increased water residence time of 8.09 ns in OH-(8,8) CNT membrane was found, whereas –CH$_3$ groups functionalization causes a reduction in water residence time of 3.11 ns. While water demonstrates a higher residence time of 7.18 ns in F-(8,8) CNT membrane. The residence time of water molecules in pristine (9,9) CNT membrane is up to 27.27 ns, demonstrating extremely low water mobility. Modification of –OH, –CH$_3$ and –F groups all lead to reduced water residence time of 7.18, 1.85 and 2.04 ns, respectively. Comparatively, in pristine (10,10) CNT membrane, the residence time for water is calculated to be 1.45 ns. In both OH-(10,10) CNT and CH$_3$-(10,10) CNT membranes, a longer residence time, 5.04 ns and
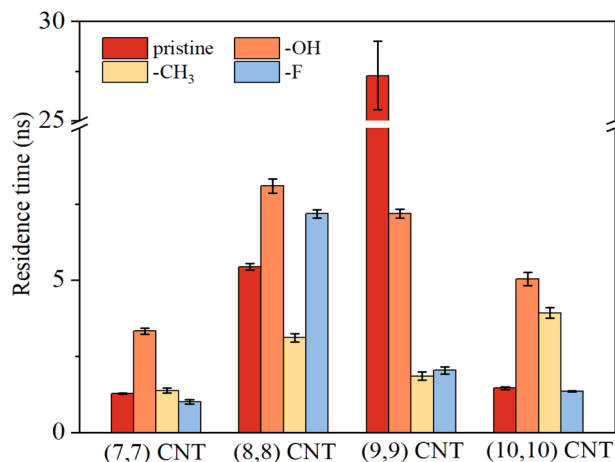
Fig. 8 Water residence time in different CNT membranes.

3.93 ns, was found; whereas water residence time is decreased to 1.35 ns in F-(10,10) CNT membrane.

The water residence time inside CNT membranes correlate with the structures of water molecules. Comparing Fig. 8 with Fig. 5, water residence time shows a similar trend as water order parameter. A long residence time corresponds to a high order parameter, indicating the low mobility of water molecules. Similarly, the residence time of water molecules in CNT membranes does not follow a monotonical increase with the pore diameter. In (8,8) and (9,9) CNTs, the highly ordered water structures cause longer water residence times. Especially for (9,9) CNT membrane, the extremely long residence time was attained. The formed hexagonal water structures in (9,9) CNT resemble ice-like configuration, displaying high viscosity and low diffusivity. Therefore, the dynamics of water molecules in (9,9) CNT membrane is extremely low, resulting in a long residence time. Correspondingly, Fig. 5c showed a significantly higher peak in the distribution curve of water order parameter for water molecules in (9,9) CNT compared with that in other CNTs, and Fig. 6c illustrated the strong water–water interaction in (9,9) CNT membrane. In addition, from Fig. S2 of ESI,† few water molecules permeate through (9,9) CNT membrane, moreover, it remained constant after 56 ns, meaning no water molecules passing through. These suggest the low dynamics and long residence time for water molecules in (9,9) CNT membrane.

Likewise, the influence of functional groups on water residence time varies for CNTs with different diameters. The –OH modification leads to an increase in water residence time in (7,7), (8,8), and (10,10) CNT membranes due to the attractions of –OH groups to water molecules, whereas, significantly decreases the residence time of water molecules in (9,9) CNT membrane because of the disruption of hexagonal water structures. –CH3 groups cause the residence time of water molecules in (7,7), (8,8), and (9,9) CNT membranes to be comparable or lower than that of the pristine CNT membranes due to the induction of more linear water structure, or the destruction of highly ordered water structures. However, the residence time of water molecules in CH3-(10,10) CNT membrane is increased, which is attributed to the emergence of

square-like water structures. Functionalizing –F groups reduces water residence time in (7,7), (9,9), and (10,10) CNT membranes, but enhances the order parameter of water molecules in (8,8) CNT membrane, resulting in an increased residence time of water molecules.

Salt rejection, water diffusion, water flow rate, water permeability

The salt rejection was examined to judge the desalination performance of the CNT membranes, as showed in Fig. 9. Additionally, the rejections of NaCl by four larger-diameter (11,11), (12,12), (13,13) and (14,14) CNT membranes were also evaluated. It was observed that all (10,10) CNT-derived membranes and CNTs with a smaller pore diameter exhibit complete retention of NaCl during 100 ns of simulations, while four CNT membranes with a larger diameter show the salt rejection rates of 98.1%, 96.2%, 92.4% and 90.5%, respectively. These demonstrate that NaCl can easily permeate through (11,11) CNT and membranes with larger pore diameters, while encounter difficulty passing through those with smaller diameters at the applied pressure.

The high rejection of NaCl by pristine CNT membranes in this study could be partly attributed to the low ΔP applied in the simulations. Some studies[36–38,82] employed an extremely high ΔP of 50–400 MPa, one or two orders of magnitude larger than the pressure applied in experiments, to simulate water desalination process in CNTs. Correspondingly, the permeation of NaCl through CNTs were observed, high water flux and low salt rejection rates were found. However, when a low ΔP, below 50 MPa, was used, the remarkably high salt rejection rates were obtained, approaching 100%, for carbon nanomembranes with a pore diameter larger than 1 nm.[83–85] Moreover, all these studies demonstrated that increasing ΔP could enlarge ion flux and reduce salt rejection. Therefore, the applied ΔP could have a significant influence on NaCl transport, and it is possible to attain a high NaCl retention rate under a low ΔP even for CNT membranes with a large pore diameter.

Furthermore, to investigate the transport behaviours of salt ions in studied CNT membranes, the radial distribution
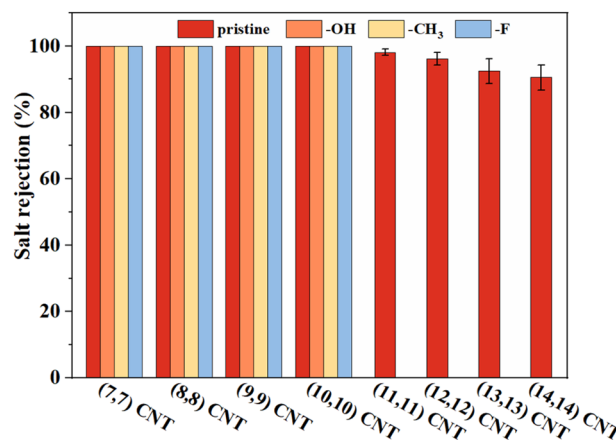

Fig. 9 Salt rejection by different CNT membranes.

functions (RDFs) for Na^+ and Cl^- ions with oxygen atoms (O_w) of water molecules were analyzed (Fig. S3 in ESI†), when they are within a distance of 0.35 nm from the entrance of CNT channels; the coordination numbers within the first hydration shells of Na^+ and Cl^- ions were calculated (Table S1 in ESI†). In addition, the number density distributions of salt ions along z coordinate were examined (Fig. S4 in ESI†). According to Fig. S3,† the peaks in Na^+–O_W and Cl^-–O_w RDF curves for Na^+ and Cl^- at the entrance of CNT membranes coincide with those in bulk water. The hydration radii of Na^+ and Cl^- ions are 0.32 nm and 0.38 nm, consistent with the results in ref. 86, corresponding to the diameters of 0.64 nm and 0.76 nm. The effective pore diameters of CNT membranes were derived from the pore volumes obtained using the Connolly surface algorithm,[41,87] as shown in Table S2.† Comparing the hydration diameters of Na^+ and Cl^- ions with the results in Table S2,† Na^+ ion might be able to cross pristine (9,9), OH-(9,9), F-(9,9) CNT and four (10,10) CNT-derived membranes, and there is a possibility for Cl^- ion traversing pristine (10,10) and OH-(10,10) CNT membranes. However, due to the Donnan exclusion effect,[88,89] the rejected Cl^- ions would attract Na^+ ions, with the results of retaining Na^+ ions as well. Therefore, the (9,9) CNT-derived, CH_3-(10,10) and F-(10,10) CNT membranes could also exhibit relatively high salt rejection. In addition, according to Fig. S3,† the RDF values of Na^+–O_w and Cl^-–O_w are merely slightly smaller than those in bulk water. The coordination numbers of Na^+ and Cl^- ions at the entrance of CNT membranes are marginally decreased compared with that in bulk water, demonstrating that the hydration structures of Na^+ and Cl^- ions remained largely undisrupted under the driving pressure. Consequently, it is also difficult for Na^+ and Cl^- ions to pass through pristine (10,10) and OH-(10,10) CNT membranes.

In addition, from Fig. S4,† it was observed that both Na^+ and Cl^- ions are distributed in saline water side for all CNT membranes studied, meaning that Na^+ and Cl^- ions were all retained in the saline water side. Moreover, the number densities of Na^+ and Cl^- ions near the entrance of CNTs are merely slightly higher than those at positions farther away, meaning a weak concentration polarization. Therefore, the concentration polarization effect induced by NaCl would produce negligible influences on water transport for studied membranes. Consequently, it would not affect water transfer simulation results.

The diffusion coefficients of water molecules in z axis $D_\perp$ in different CNT membranes are shown in Fig. 10a. The numbers of water molecules N_w transferred through different CNT membranes from the saline water side to the pure water side were counted (see Fig. S2 of ESI†). It was observed that N_w increases linearly with simulation time within 100 ns for almost all membranes, except for pristine (9,9) CNT membrane, which is due to the formation of ice-like water structure that significantly reduce water dynamics, indicating a steady-state of water flow. The N_w is much lower than the initial number of water molecules in the saline box for all CNT membranes, which means that the salt solution side would not be drained within 100 ns. The final snapshot of F-(10,10) CNT membrane where the largest number of water molecules passing through was shown in Fig. S5 of ESI.† It was observed that there were still lots
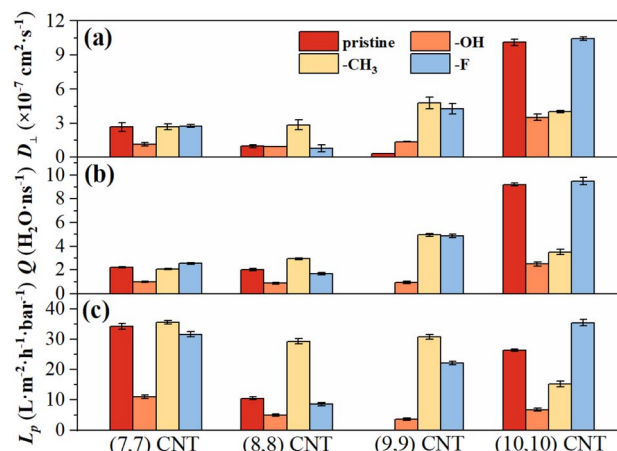

Fig. 10 Water diffusion coefficient in z direction (a), water flow rate (b) and water permeability (c) in different CNT membranes.

of water molecules in the salt solution side. The water flow rate Q was calculated by fitting the slope of N_w vs. simulation time curve, as shown in Fig. 10b. Water permeability L_p is further analysed by the equation $L_p = Q/[A(\Delta P - \Delta\pi)]$,[90] where A is the pore area, $\Delta\pi$ is the osmotic pressure of the salt solution. The value of $\Delta\pi$ for 32 000 mg L^{-1} NaCl is 25.2 bar.[91] The results are presented in Fig. 10c.

The hierarchy of water perpendicular diffusion coefficient, water flow rate and water permeability for different CNT membranes are consistent. As seen in Fig. 10a, $D_\perp$ in pristine (7,7) CNT is ca. 2.65×10^{-7} cm^2 s^{-1}, correspondingly, the calculated Q and L_p are 2.22 H_2O ns^{-1} and 34.3 L m^{-2} h bar^{-1}, respectively. The –OH functionalization causes a reduction in $D_\perp$, Q and L_p, which is attributed to the increased tetrahedrality of water molecules (Fig. 5a) and HBs between –OH groups and water molecules that enhance surface friction. Comparatively, a slightly higher $D_\perp$ value was observed both in CH_3-(7,7) CNT and F-(7,7) CNT membranes due to the decreased tetrahedrality. Although there is lower Q, due to the significant reduction of effective pore diameter (Table S2†), the CH_3-(7,7) CNT membrane even exhibits a higher L_p of 35.6 L m^{-2} h bar^{-1} than that of the pristine (7,7) CNT. While F-(7,7) CNT membrane has a lower L_p but with a larger Q.

The $D_\perp$ for water molecules in pristine (8,8) CNT membrane is decreased to 0.96×10^{-7} cm^2 s^{-1}, which is because of the formation of square-like water structure in pristine (8,8) CNT that significantly enhances the tetrahedral order of water molecules and strengthens water–water interaction. The calculated Q and L_p are also smaller than those of pristine (7,7) CNT membrane. Similarly, modification with –OH groups lowers $D_\perp$, Q, as well as L_p but with decreased tetrahedral order, demonstrating that the hydrogen bonding between –OH and water molecules plays a more important role in water transport. In contrast, –CH_3 functionalization increases $D_\perp$, Q and L_p due to the breakage of ordered square-like structure. While the $D_\perp$, Q and L_p for water molecules in F-(8,8) CNT membrane all becomes smaller because of increased tetrahedrality of water structure.

Paper

From Fig. 10a, the pristine (9,9) CNT membrane exhibits an extremely low $D_\perp$, 0.33×10^{-7} cm^2 s^{-1}, Q and L_p both approach zero, which is due to formation of hexagonal-like water structure (Fig. 2c), which is consistent with the result in ref. 69, that water diffusion showed a minimum in (9,9) CNT. Addition of –OH, –CH$_3$ and –F groups all cause an increased $D_\perp$, as well as Q and L_p because of the disruption of the highly ordered water structure. This also indicates that the enhancement of water transport by decreased tetrahedral order counteracts the surface friction effect by HBs between –OH groups with water molecules in OH-(9,9) CNT membrane.

For pristine (10,10) CNT membrane, the values of $D_\perp$, Q and L_p are 10.1×10^{-7} cm^2 s^{-1}, 9.23 H$_2$O ns^{-1} and 26.3 L m^{-2} h bar^{-1}, respectively. These three parameters are all significantly decreased in OH-(10,10) CNT because of the surface friction effect. The reduced values of $D_\perp$, Q and L_p were also observed in CH$_3$-(10,10) CNT due to the appearance of ice-like water molecules. However, the $D_\perp$ is increased to 10.4×10^{-7} cm^2 s^{-1} for water molecules in F-(10,10) CNT membrane; the Q and L_p also become larger, which is attributed to the decreased tetrahedrality. Generally, through changing channel diameter and functionalization, the system with the low tetrahedral order corresponds to more single-file-like water structure, and is associated with rapid water diffusion and high water permeance; while systems with increased tetrahedrality results in more ice-like water structure, and have a lower water diffusion coefficient and permeability.

Conclusions

In this work, the MD simulation method was utilized to investigate water transport mechanism in nanochannels in a desalination process, CNTs with different diameters were used as the model nanochannels and the effect of different modification with –OH, –CH$_3$ and –F groups was investigated. Our simulation results showed that water transport in nanochannel significantly depends on the confined water structure. Small diameter (7,7) CNT allows the single-file-like water transport mode. Increasing CNT diameter, water structures are changed into square and hexagonal-like in (8,8) and (9,9) CNT membranes, then a disordered structure in (10,10) CNT, resulting in a concave-shaped trend of water permeance. Functionalizing –OH groups increases tetrahedral order of water molecules in (7,7) CNT, while disrupts the highly tetrahedral water structure in (8,8) and (9,9) CNT membrane, and reduces the degree of order in (10,10) CNT, meanwhile, enhances surface friction for water transport. The damage of ordered water structure in OH-(9,9) CNT results in significantly improved water permeance; while the friction effect plays a more important role in OH-(8,8) and OH-(10,10) CNT membranes, leading to reduced water transport. The –CH$_3$ groups decreases the tetrahedrality of water structures, that causes more stricter single-file water arrangement in CH$_3$-(7,7) CNT, changes water structures into two-column and triangular arrangements in CH$_3$-(8,8) and CH$_3$-(9,9) CNT membranes, which enhances water transport; while increased tetrahedral order and unexpected square structure are found in CH$_3$-(10,10) CNT membrane. The fluorination of CNT reduces the degree of

tetrahedrality of water molecules in F-(7,7), F-(9,9) and F-(10,10) CNT membranes, resulting in a higher water permeance; however, the increased tetrahedral order and square water structure are found in F-(8,8) CNT. The results of this study demonstrate that the transport of water molecules within nanochannels depends on water structure, which could be modulated precisely by controlling channel diameter and chemical functionalization. Reducing the tetrahedral order of water molecules results in more single-file-like water structure, corresponding to rapid water diffusion and high water permeance; an increase in water tetrahedrality leads to more ice-like water structure, associated with a lower water diffusion coefficient and permeability. In the molecular design of artificial nanochannels, such as for desalination or ion sieving, it is crucial to devise appropriate pore sizes, select suitable functional groups and modification sites to avoid forming ice-like structures or disrupting the existing ordered water structures through rational modifications to achieve fast water transport.

Author contributions

Lanlan Qin: methodology, software, validation, formal analysis, investigation, data curation, writing – original draft, visualization, funding acquisition. Jian Zhou: conceptualization, resources, writing – review & editing, supervision, project administration, funding acquisition.

Conflicts of interest

There are no conflicts to declare.

Acknowledgements

References

1 Y. Hoekstra Arjen and O. Wiedmann Thomas, *Science*, 2014, **344**, 1114–1117.
2 J. Eliasson, *Nature*, 2015, **517**, 6.
3 M. M. Mekonnen and A. Y. Hoekstra, *Sci. Adv.*, 2016, **2**, e1500323.
4 M. Kamali, D. P. Suhas, M. E. Costa, I. Capela and T. M. Aminabhavi, *Chem. Eng. J.*, 2019, **368**, 474–494.
5 P. S. Goh, T. Matsuura, A. F. Ismail and N. Hilal, *Desalination*, 2016, **391**, 43–60.
6 L. F. Greenlee, D. F. Lawler, B. D. Freeman, B. Marrot and P. Moulin, *Water Res.*, 2009, **43**, 2317–2348.
7 M. Elimelech and W. A. Phillip, *Science*, 2011, **333**, 712–717.
8 A. Doyle Declan, M. Cabral João, A. Pfuetzner Richard, A. Kuo, M. Gulbis Jacqueline, L. Cohen Steven, T. Chait Brian and R. MacKinnon, *Science*, 1998, **280**, 69–77.
9 K. Murata, K. Mitsuoka, T. Hirai, T. Walz, P. Agre, J. B. Heymann, A. Engel and Y. Fujiyoshi, *Nature*, 2000, **407**, 599–605.

10 R. MacKinnon, *Angew. Chem., Int. Ed.*, 2004, **43**, 4265–4277.

11 C. Y. Tang, Y. Zhao, R. Wang, C. Hélix-Nielsen and A. G. Fane, *Desalination*, 2013, **308**, 34–40.

12 J. Habel, M. Hansen, S. Kynde, N. Larsen, S. R. Midtgaard, G. V. Jensen, J. Bomholt, A. Ogbonna, K. Almdal, A. Schulz and C. Hélix-Nielsen, *Membranes*, 2015, **5**, 307–351.

13 L. Chen, W. Si, L. Zhang, G. Tang, Z.-T. Li and J.-L. Hou, *J. Am. Chem. Soc.*, 2013, **135**, 2152–2155.

14 H. Tunuguntla Ramya, Y. Henley Robert, Y.-C. Yao, A. Pham Tuan, M. Wanunu and A. Noy, *Science*, 2017, **357**, 792–796.

15 L. Qin, H. Huang and J. Zhou, *Mol. Simul.*, 2023, **49**, 1742–1757.

16 W. Song, H. Joshi, R. Chowdhury, J. S. Najem, Y.-x. Shen, C. Lang, C. B. Henderson, Y.-M. Tu, M. Farell, M. E. Pitz, C. D. Maranas, P. S. Cremer, R. J. Hickey, S. A. Sarles, J.-l. Hou, A. Aksimentiev and M. Kumar, *Nat. Nanotechnol.*, 2020, **15**, 73–79.

17 Y. D. Yuan, J. Dong, J. Liu, D. Zhao, H. Wu, W. Zhou, H. X. Gan, Y. W. Tong, J. Jiang and D. Zhao, *Nat. Commun.*, 2020, **11**, 1–10.

18 M. Di Vincenzo, A. Tiraferri, V.-E. Musteata, S. Chisca, R. Sougrat, L.-B. Huang, S. P. Nunes and M. Barboiu, *Nat. Nanotechnol.*, 2021, **16**, 190–196.

19 L.-B. Huang, A. Hardiagon, I. Kocsis, C.-A. Jegu, M. Deleanu, A. Gilles, A. van der Lee, F. Sterpone, M. Baaden and M. Barboiu, *J. Am. Chem. Soc.*, 2021, **143**, 4224–4233.

20 A. Roy, J. Shen, H. Joshi, W. Song, Y.-M. Tu, R. Chowdhury, R. Ye, N. Li, C. Ren and M. Kumar, *Nat. Nanotechnol.*, 2021, **16**, 911–917.

21 Z. Xu, Z. He, X. Quan, D. Sun, Z. Miao, H. Yu, S. Yang, Z. Chen, J. Zeng and J. Zhou, *Chin. J. Chem. Eng.*, 2021, **31**, 206–226.

22 Z. He, J. Zhou, X. Lu and B. Corry, *ACS Nano*, 2013, **7**, 10148–10157.

23 Y. Zhu, Y. Ruan, Y. Zhang, Y. Chen, X. Lu and L. Lu, *Langmuir*, 2017, **33**, 9201–9210.

24 R. J. Mashl, S. Joseph, N. R. Aluru and E. Jakobsson, *Nano Lett.*, 2003, **3**, 589–592.

25 T. A. Pascal, W. A. Goddard and Y. Jung, *Proc. Natl. Acad. Sci. U. S. A.*, 2011, **108**, 11794–11798.

26 L. Wang, R. S. Dumont and J. M. Dickson, *J. Chem. Phys.*, 2013, **138**, 124701.

27 T. Tajiri, R. Matsuzaki and Y. Shimamura, *Sci. Rep.*, 2016, **6**, 32262.

28 M. Rezaee, H. Ghassemi and S. Jabari Neek, *Mater. Today Commun.*, 2023, **37**, 107188.

29 J. Shen, R. Ye, A. Romanies, A. Roy, F. Chen, C. Ren, Z. Liu and H. Zeng, *J. Am. Chem. Soc.*, 2020, **142**, 10050–10058.

30 A. Horner, F. Zocher, J. Preiner, N. Ollinger, C. Siligan, S. A. Akimov and P. Pohl, *Sci. Adv.*, 2015, **1**, e1400083.

31 B. Corry, *J. Phys. Chem. B*, 2008, **112**, 1427–1434.

32 M. Majumder, N. Chopra and B. J. Hinds, *J. Am. Chem. Soc.*, 2005, **127**, 9062–9070.

33 B. Corry, *Energy Environ. Sci.*, 2011, **4**, 751–759.

34 W.-F. Chan, H.-y. Chen, A. Surapathi, M. G. Taylor, X. Shao, E. Marand and J. K. Johnson, *ACS Nano*, 2013, **7**, 5308–5319.

35 P. S. Goh, A. F. Ismail and N. Hilal, *Desalination*, 2016, **380**, 100–104.

36 S. J. Mahdizadeh, E. K. Goharshadi and G. Akhlamadi, *Phys. Chem. Chem. Phys.*, 2018, **20**, 22241–22248.

37 D. Yang, Q. Li, J. Shi, J. Wang and Q. Liu, *New J. Chem.*, 2017, **41**, 14325–14333.

38 C. Ding and J. Su, *Appl. Surf. Sci.*, 2023, **607**, 154971.

39 C. Ding, Y. Zhao and J. Su, *Langmuir*, 2021, **37**, 12318–12326.

40 W. Tian, Y. Bao, G. Qin, L. Liu and X. Zheng, *J. Mol. Liq.*, 2023, **392**, 123433.

41 S. Velioğlu, H. E. Karahan, K. Goh, T.-H. Bae, Y. Chen and J. W. Chew, *Small*, 2020, **16**, 1907575.

42 M. Divandari, A. Arcifa, M. A. Ayer, C. Letondor and N. D. Spencer, *Langmuir*, 2021, **37**, 4387–4394.

43 Z. Wu, L. Tang, J. Dai and J. Qu, *J. Coat. Technol. Res.*, 2019, **16**, 1233–1241.

44 L. Wang, R. S. Dumont and J. M. Dickson, *Mol. Phys.*, 2017, **115**, 981–990.

45 H. Zhang, M. S. Wu, K. Zhou and A. W.-K. Law, *Environ. Sci. Technol.*, 2019, **53**, 6374–6382.

46 M. J. Abraham, T. Murtola, R. Schulz, S. Páll, J. C. Smith, B. Hess and E. Lindahl, *SoftwareX*, 2015, **1–2**, 19–25.

47 W. L. Jorgensen, D. S. Maxwell and J. Tirado-Rives, *J. Am. Chem. Soc.*, 1996, **118**, 11225–11236.

48 H. J. C. Berendsen, J. R. Grigera and T. P. Straatsma, *J. Phys. Chem.*, 1987, **91**, 6269–6271.

49 T. Darden, D. York and L. Pedersen, *J. Chem. Phys.*, 1993, **98**, 10089–10092.

50 W. G. Hoover, *Phys. Rev. A*, 1985, **31**, 1695–1697.

51 Z. He, J. Zhou, X. Lu and B. Corry, *J. Phys. Chem. C*, 2013, **117**, 11412–11420.

52 H. Zhang, H. Ye, Y. Zheng and Z. Zhang, *Microfluid. Nanofluid.*, 2011, **10**, 403–414.

53 H. Ye, H. Zhang, Y. Zheng and Z. Zhang, *Microfluid. Nanofluid.*, 2011, **10**, 1359–1364.

54 J. Zhou and W. Wang, *Langmuir*, 2000, **16**, 8063–8070.

55 M. H. Köhler and L. B. da Silva, *Chem. Phys. Lett.*, 2016, **645**, 38–41.

56 C. Chen, L. Jia, J. Li, L. Zhang, L. Liang, E. Chen, Z. Kong, X. Wang, W. Zhang and J.-W. Shen, *Desalination*, 2020, **491**, 114560.

57 M.-J. Wei, J. Zhou, X. Lu, Y. Zhu, W. Liu, L. Lu and L. Zhang, *Fluid Phase Equilib.*, 2011, **302**, 316–320.

58 L.-L. Huang, L.-Z. Zhang, Q. Shao, J. Wang, L.-H. Lu, X.-H. Lu, S.-Y. Jiang and W.-F. Shen, *J. Phys. Chem. B*, 2006, **110**, 25761–25768.

59 H. Dai, Z. Xu and X. Yang, *J. Phys. Chem. C*, 2016, **120**, 22585–22596.

60 A. Noy, H. G. Park, F. Fornasiero, J. K. Holt, C. P. Grigoropoulos and O. Bakajin, *Nano today*, 2007, **2**, 22–29.

61 J. Wang, Y. Zhu, J. Zhou and X.-H. Lu, *Phys. Chem. Chem. Phys.*, 2004, **6**, 829–835.

62 R. M. Pashley and J. N. Israelachvili, *J. Colloid Interface Sci.*, 1984, **101**, 511–523.

63 B. Zobrist, V. Soonsin, B. P. Luo, U. K. Krieger, C. Marcolli, T. Peter and T. Koop, *Phys. Chem. Chem. Phys.*, 2011, **13**, 3514–3526.

64 M. Ferrario, M. Haughney, I. R. McDonald and M. L. Klein, *J. Chem. Phys.*, 1990, **93**, 5156–5166.

65 J. Zheng, L. Li, S. Chen and S. Jiang, *Langmuir*, 2004, **20**, 8931–8938.

66 B. Mukherjee, P. K. Maiti, C. Dasgupta and A. K. Sood, *ACS Nano*, 2010, **4**, 985–991.

67 D. Cohen-Tanugi and J. C. Grossman, *Nano Lett.*, 2012, **12**, 3602–3608.

68 K. Koga, G. T. Gao, H. Tanaka and X. C. Zeng, *Nature*, 2001, **412**, 802–805.

69 M. Kuehne, S. Faucher, M. Liew, Z. Yuan, S. X. Li, T. Ichihara, Y. Zeng, P. Gordiichuk, V. B. Koman, D. Kozawa, A. Majumdar and M. S. Strano, *J. Phys. Chem. C*, 2021, **125**, 25717–25728.

70 Y. Liu, Q. Wang, L. Zhang and T. Wu, *Langmuir*, 2005, **21**, 12025–12030.

71 M. Fulford, M. Salvalaglio and C. Molteni, *J. Chem. Inf. Model.*, 2019, **59**, 2141–2149.

72 J. R. Errington and P. G. Debenedetti, *Nature*, 2001, **409**, 318–321.

73 Z. Kong, P. Zhang, X. Ma, H. Zhou, L. Liang, J.-W. Shen and H. Wang, *Chem. Phys.*, 2020, **538**, 110887.

74 G. Zuo, R. Shen, S. Ma and W. Guo, *ACS Nano*, 2010, **4**, 205–210.

75 A. Horner, C. Siligan, A. Cornean and P. Pohl, *Faraday Discuss.*, 2018, **209**, 55–65.

76 M. Sadakiyo, T. Yamada and H. Kitagawa, *J. Am. Chem. Soc.*, 2011, **133**, 11050–11053.

77 W. Zhang, M. Shi, Z. Heng, W. Zhang and B. Pan, *Nano Lett.*, 2020, **20**, 7327–7332.

78 N. Wei, X. Peng and Z. Xu, *ACS Appl. Mater. Interfaces*, 2014, **6**, 5877–5883.

79 T. Xu, M. Zhang, Z. Xu and X. Yang, *ACS Appl. Mater. Interfaces*, 2019, **11**, 33409–33418.

80 L. Qin, H. Huang and J. Zhou, *Mol. Simul.*, 2023, **49**, 1742–1757.

81 Y. He, J. Hower, S. Chen, M. T. Bernards, Y. Chang and S. Jiang, *Langmuir*, 2008, **24**, 10358–10364.

82 M. Abbaspour, M. Namayandeh Jorabchi and H. Akbarzadeh, *J. Mol. Liq.*, 2023, **384**, 122310.

83 Y. Wang, Z. He, K. M. Gupta, Q. Shi and R. Lu, *Carbon*, 2017, **116**, 120–127.

84 M. Hosseini, J. Azamat and H. Erfan-Niya, *Appl. Surf. Sci.*, 2018, **427**, 1000–1008.

85 M. Hosseini, J. Azamat and H. Erfan-Niya, *Mater. Chem. Phys.*, 2019, **223**, 277–286.

86 J. Zhou, X. Lu, Y. Wang and J. Shi, *Fluid Phase Equilib.*, 2002, **194–197**, 257–270.

87 M. Mehrdad and A. Moosavi, *Polymer*, 2019, **175**, 310–319.

88 J. Schaep, B. Van der Bruggen, C. Vandecasteele and D. Wilms, *Sep. Purif. Technol.*, 1998, **14**, 155–162.

89 Y. Han, Z. Xu and C. Gao, *Adv. Funct. Mater.*, 2013, **23**, 3693–3700.

90 Y. J. Lim, K. Goh, M. Kurihara and R. Wang, *J. Membr. Sci.*, 2021, **629**, 119292.

91 https://www.lenntech.com/products/membrane/lg-chem.htm.